

Correction of Field Rotator-Induced Flat-Field Systematics - A Case Study Using Archived VLT-FORS Data

Sabine Moehler, Wolfram Freudling, Palle Møller, Ferdinando Patat, Gero Rupprecht
European Southern Observatory, Karl-Schwarzschild-Str. 2, D-85748 Garching bei München, Germany

Kieran O'Brien
European Southern Observatory, Casilla 19001, Santiago 19, Chile
 smoehler,wfreudli,pmoller,fpatat,grupprec,kobrien@eso.org

ABSTRACT

ESO's two **FO**cal **R**educer and low dispersion **S**pectrographs (FORS) are the primary optical imaging instruments for the VLT. They are not direct-imaging instruments, as there are several optical elements in the light path. In particular, both instruments are attached to a field rotator. Obtaining truly photometric data with such instruments present a significant challenge. In this paper, we investigate in detail twilight flats taken with the FORS instruments. We find that a large fraction of the structure seen in these flatfields rotates with the field rotator.

We discuss in detail the methods we use to determine the cause of this effect. The effect was tracked down to be caused by the Linear Atmospheric Dispersion Corrector (LADC). The results are thus of special interest for designers of instruments with LADCs and developers of calibration plans and pipelines for such instruments. The methods described here to find and correct it, however, are of interest also for other instruments using a field rotator.

If not properly corrected, this structure in the flatfield may degrade the photometric accuracy of imaging observations taken with the FORS instruments by adding a systematic error of up to 4% for broad band filters. We discuss several strategies to obtain photometric images in the presence of rotating flatfield pattern.

Subject headings: Astronomical Instrumentation

1. Introduction

Systematic differences between flat field images, i.e. high count level CCD exposures of a smooth/diffuse source, and the actual system efficiency at any position of the CCD ultimately set a limit for the photometric accuracy of an imaging instrument unless they are accurately determined and corrected for. This correction process is known as “illumination correction” and is especially important for focal reducer type instruments due to their numerous internal reflections that redistribute diffuse light, an effect sometimes referred to as “sky concentration” (see for instance Andersen et al. 1995; Koch et al. 2003).

The two optical focal reducer instruments FORS1 and FORS2 have been in operation at the ESO VLT since April 1, 1999, and April 1, 2000, respectively. During this time a large database of calibration data has been accumulated. In an effort to improve the overall photometric accuracy that we offer to ESO users, we are in the process of defining a procedure to determine and correct for systematics such as sky concentration (Møller et al. 2005; Freudling et al. 2007a,b).

In the course of this work we have found an effect that has previously not been described in the literature. The effect is seen as twilight image features that rotate along with the field rotator position and therefore clearly are created

inside the telescope/instrument system. The effect might not be limited to the two FORS instruments, but affect other instruments mounted on telescopes with field rotators. Due to our vast database covering about one decade of systematically obtained and documented calibration data we are able to investigate and quantify the features.

The paper is organized in the following way. In Sec. 2, we describe the selection and processing of the data used in this investigation. In Sec. 3, we describe how we isolated the rotating part of the flat fields and investigate the properties and origin of this structure. Finally, in Sec. 4, we discuss the impact of our finding on photometry and strategies for dealing with this effect.

2. Data

The current calibration plan for the FORS instruments specifies that twilight flat fields have to be taken within seven nights of a science observation with a given setup. Usually about 4–6 frames are taken, mostly during evening twilight, but sometimes also during morning twilight. Hereafter, we refer to these individual images as “twilight flats”. In order to eliminate the contributions of field stars on the jittered sequence of flat fields, the frames are combined using a median rather than a simple average. Before combining the individual frames, the master bias is subtracted and each frame is normalized with the median of its flux. The resulting masterflats are used for the pipeline processing of the images and also by most users of FORS data.

We used the individual twilight flats to investigate the properties of flatfields taken with the FORS instruments. For that purpose, we retrieved data from the ESO archive observed between April 1, 1999 and April 11, 2008 for FORS1 and between May 1, 2000 and November 1, 2008 for FORS2. Within these time intervals, the FORS instruments and the telescopes they were attached to went through several maintenance intervals and/or upgrades, and the instruments were moved to different Unit Telescopes (UTs) of the VLT. In order to assess the stability of the twilight flats, we took care to combine only twilight flats taken between such interventions. The periods we considered are detailed in Table 1. In addition to

the archive data from the calibration plan, we obtained a specifically designed sequence of twilight flats for FORS1 with the OII+44 filter between August 31 and September 4, 2007. This filter is an interference filter centered at 372 nm. These observations are the only ones that were explicitly taken to analyze the rotating feature and the rotator angle was changed in roughly 10° steps.

Before investigating the flatfields in more detail, we prepared them in the following way. First, each individual image was bias-corrected using the pre-scan region only and normalized with the median of its flux (hereafter flux-normalized twilight flat). The single CCDs of the FORS instruments were read out via four ports in standard imaging mode, that yields different gains for the four quadrants (see the FORS manual¹ for more details). In these cases the median was determined from the region from 100,100 (lower left corner) to 900,900 (upper right corner), covering the first quadrant of the CCD. For the CCD mosaics we first combined the 2 frames corresponding to one exposure and extracted the illuminated part. Within the illuminated part the flux was determined for the region 500,900 (lower left corner) to 800,1500 (upper right corner).

A cursory inspection of the flux-normalized flatfields shows that individual flats differ by as much as 5% in amplitude. At the same time, there is a stable component that is similar for all twilight flats for a given time range between interventions. This stable component emerges when the median of those twilight flats is computed and is often dominated by sky light concentration (see Fig. 1). In Fig. 2, the shape of the pattern is shown for the broad band and the narrow band filter we used. The figure shows cuts through the medians for the Bessell U, B, V, R and I filters and the OII narrow band filter. The overall shape and amplitude is similar for all filters, and the total amplitude is on the order of 3 to 5%.

In order to investigate the changing component of the twilight flats, we divided each flat by the median flux-normalized twilight flat for the corresponding filter (hereafter flatfielded twilight flat). This removes any structure of the flatfield which is stable and fixed relative to the detector.

¹<http://www.eso.org/sci/facilities/paranal/instruments/fors/doc/>

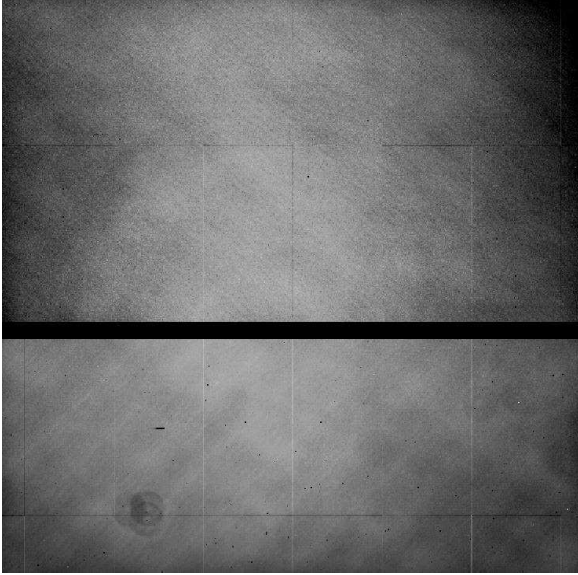


Fig. 1.— The median of the flux-normalized FORS1 *R* twilight flat fields at UT2 during the time range from 2007-04-01 to 2007-09-24 with the two CCDs corrected to the same flux level at $50''$ distance from the center of the field. The cuts are at 0.95 and 1.05.

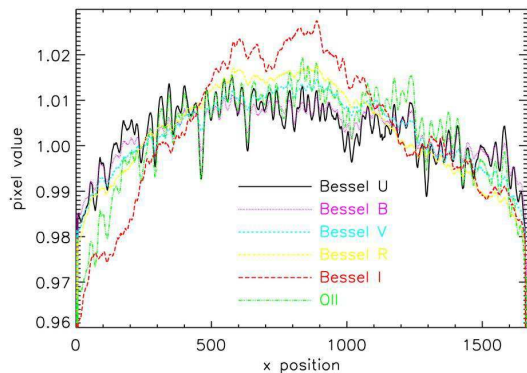


Fig. 2.— Horizontal cuts across the flux-normalized median twilight flats taken with FORS1 from 2007-04-01 to 2007-09-24.

3. Changing Component of Twilight Flats

3.1. Rotating Pattern

Inspection of the flatfielded twilight flats revealed that some of the remaining structures seem to change their position between flatfields taken in the same night. This observation immediately rules out that these features are caused by spatial sensitivity variations on the detector, or vignetting on structures which are physically fixed relative to the detector. Instead, at least some of the variations in the flatfields must be caused by moving parts within the telescope or FORS instrument. The alt/az mounting of the VLT UT telescopes causes field rotation, which is compensated by rotating the instrument accordingly. Fixed components along the light path (e.g. the Linear Atmospheric Dispersion Corrector or the M3) will therefore rotate with respect to the detector of the instrument. To test whether the flatfield structures are related to the field rotation, we compared twilight flats taken with different rotator angles.

In order to investigate the exact relation between the orientation of structures in the twilight flats and that of the field rotator, we took a set of twilight images with a maximum of 5 images per 5° interval in rotator angle. These were then counter rotated with the angle of the field rotator multiplied with a factor ϵ between 0 and 2. Then we computed the median of these counter rotated flatfielded twilight flats and measured the amplitude of the structures as the difference between the 99th and 1st percentile. Only pixels within a centered circle with a diameter equal to the dimension of the image were used for that purpose. The amplitudes as a function of the rotation factor ϵ are shown in Fig. 3. It can be seen that the amplitudes of structures peak when the de-rotation angle is exactly identical to the rotator angle. We therefore use rotations with the opposite of the exact rotator angle to isolate the rotating pattern (hereafter RP).

We applied this procedure to the data sets described in Table 1. We compared the structures in the resulting image with the median of the same frames, but rotated by a random rotation angle. One example of such a comparison is shown in Fig. 4. The amplitude of structures in the median of the counter rotated flatfielded frames is typically between about 0.6% and 2.0%, whereas

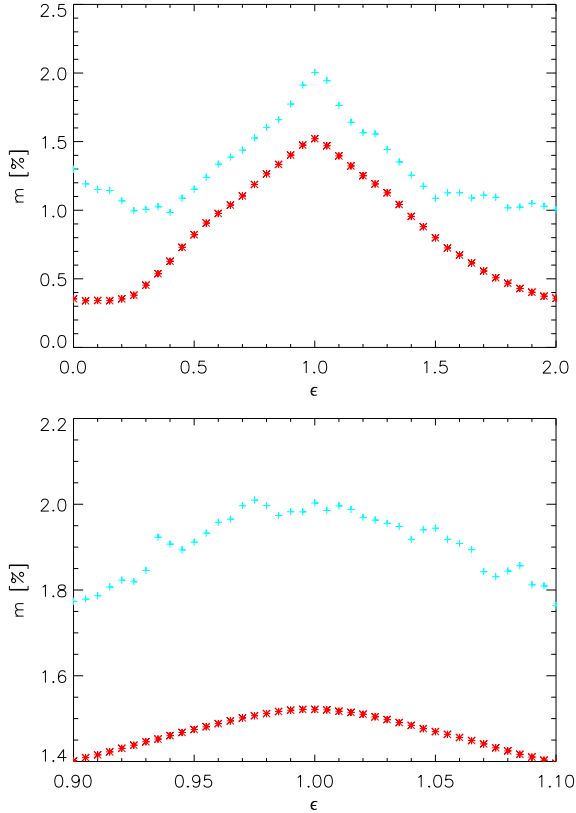


Fig. 3.— Amplitudes measured in the median of rotated flatfielded twilight flats as a function of rotation factor. Crosses (+) are the differences between maximum and minimum pixel values for each rotation angle, whereas the stars are the amplitudes of structures estimated as the difference between the 99th and 1st percentiles. A rotation factor of unity indicates that each flatfield has been rotated by the negative of the rotator angle. The top panel show the whole range of values for ϵ , while the lower panel zooms in on the peak of the distribution. For this test we used the data set FORS1@UT1, 2000-08-01 to 2001-02-25.

no structure can be recognized in the median of randomly rotated flatfielded frames.

So far, we have identified two components of the flatfields, one is the pattern fixed relative to the detector, and the other one is the RP. An interesting question is on what scales the RP becomes relevant, and whether all structure in the flatfield which is not fixed to the detector can be attributed to the RP. To investigate this, we computed the power spectrum within the central circle of the isolated RP, and divided it by the power spectrum of the same region in the randomly rotated average. The result is shown as crosses (+) in Fig. 5. It can be seen that the range of scales present in the RP is from about 30 pixels to the size of the CCD. This power spectrum should be compared to that in a flatfield with a single rotator angle. For that purpose, the power spectrum of twilight flats with rotator angles between 135° and 145°, is shown as triangles in Fig. 5. A comparison of these two power spectra reveals that the structure in the flatfields at scales above about 300 pixels is dominated by the RP. At intermediate scales between 30 and 300 pixels, the amplitude of the RP is small compared to other structure in the flatfield. To illustrate this more clearly, we removed the RP from the individual flatfielded flats with rotator angles between 135° and 145° after rotating it in place, and then computed the average. The power spectra of the RP corrected average flatfielded flat are shown as squares in Fig. 5. It can be seen that most of the power at scales larger than 300 pixels can be removed when correcting the isolated RP at the correct rotator angle.

3.2. Rotating Pattern for different filters

The next question we wish to address is whether the shape and amplitude of the RP depend on the filter. We therefore isolated the RP with the method described in Sect 3.1 for all filters within the periods that include a sufficient number of narrow band observations. In Fig. 6, we show the RPs for one of these periods. It is clearly seen that the amplitude as well as the shape of the structure vary smoothly with wavelength for the broad band filters. The amplitudes for different filters are listed Tab. 2, and the variation in amplitude are illustrated in Fig. 7. The amplitudes are about 1.8% for the narrow-band filter, and below 1.5% for the broadband filters. This trend has to be

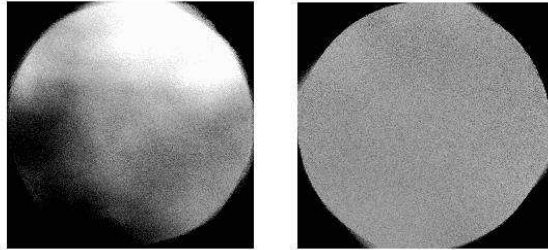


Fig. 4.— **Left:** The median of the flatfielded FORS1 *B* twilight flat fields rotated to rotator angle of 0 at UT1 during the time range from 2000-08-01 to 2001-02-25. **Right:** Same as in left panel, but with the individual images rotated to random rotator angles. Both images are displayed with cuts of 0.995 and 1.005.

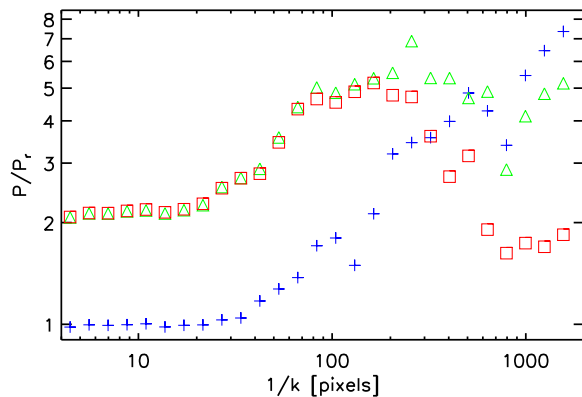


Fig. 5.— Normalized power spectra as a function of scale length derived from a flatfielded twilight flat field, that has been corrected for the stable component (same data set as for Fig. 3). The crosses (+) represent the power spectrum of the RP, the triangles that of the average of twilight flats with the same rotator angle, and the squares of the average with the RP removed (see text). All power spectra were computed within the central circle on the images, and divided by the power spectrum of the randomly rotated average.

considered when searching for the cause of the RP (see Sec. 4.1).

This larger amplitude of the RP seen in the narrow band filters means that more photons were detected in the RP relative to photons detected in the underlying twilight image. One possible way to explain this is that while the underlying image only detects photons within the passbands of the narrow band filters, the RP is made up of photons that do not pass through the filter and therefore has the full bandwidth of unfiltered twilight. This explanation implies a correlation of the amplitude with the fraction of photons that pass through the filter. Such an effect has been reported by Fynbo et al. (1999) for narrow band observations at the NOT telescope. This fraction of sky photons that pass through a filter can be computed from the width of the filter bandpass, the mean transmission of the filter, the mean CCD efficiency over the bandpass, the relative brightness of the twilight sky within the bandpass and the total sky brightness and exposure time. To estimate this number, we used the twilight sky brightness at different bandpasses from Patat et al. (2006), and the filter and CCD characteristics for FORS, which are available on the World Wide Web².

We then computed the ratio r of the number of photons available outside the filter to the number of photons detected after passing through the filter as

$$r = \frac{\int N_p(\lambda) f(\lambda) d\lambda}{\int N_p(\lambda) d\lambda} \quad (1)$$

where $N_p(\lambda)$ is the detected photon rate as a function of wavelength, and $f(\lambda)$ is the filter throughput curve. The photon rate was computed from

$$N_p(\lambda) = S(\lambda) \cdot R_{\text{CCD}}(\lambda) \quad (2)$$

where $S(\lambda)$ is the twilight sky brightness expressed in photons per wavelength, and $R_{\text{CCD}}(\lambda)$ is the response of the CCD.

In Fig. 8, we plot the measured amplitude of the RP versus the fraction of sky photons that pass through the filter. It can be seen that there is some trend in the sense that a when only a small

²<http://www.eso.org/sci/facilities/paranal/instruments/fors/inst/>

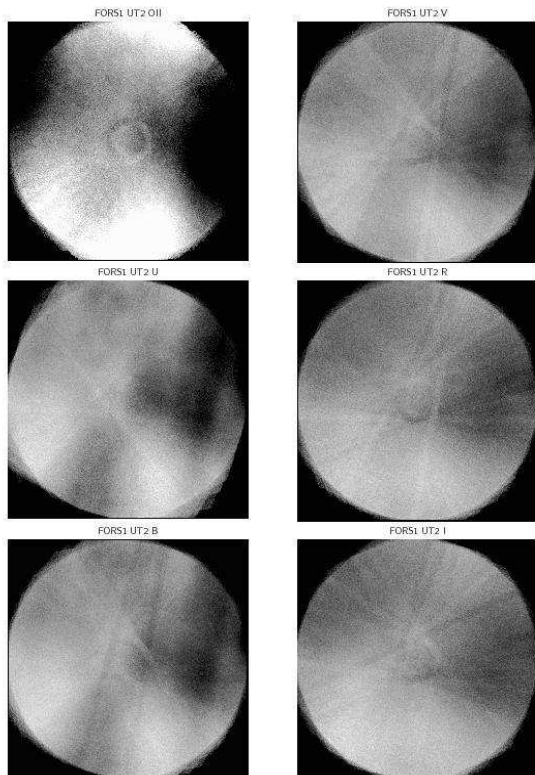


Fig. 6.— Comparison of flatfielded twilight flat fields rotated to rotator angle 0 for the broad-band filters UBVR_I and the narrow-band filter OII observed with FORS1 at UT2 from 2007-04-01 to 2007-09-24. All images are displayed with cuts of 0.995 and 1.005. See text for further details.

fraction of the photons pass through the filter, the amplitudes tend to be higher. However, the large scatter make this test inclusive. In Sec. 4, we will discuss a more sensitive test to determine whether the RP is likely to be caused by scattering.

3.3. Stability of Rotating Pattern

The finding that some of the structures in twilight flats rotate with the rotator angle has significant impact on the photometry with either of the FORS instruments. To correct for this effect, it is important to know how stable this pattern is with time. Both instruments have been moved between the telescopes which comprise the four unit VLT. Both FORSs use Linear Atmospheric Dispersion Correctors (Avila, Rupprecht & Beckers 1997, LADCs) which are fixed to the telescope and mounted in front of the instrument. The two existing LADCs, called LADC-A and LADC-B, have also been switched between the two FORSs once (June 2004). The different combinations of LADCs, telescopes and instruments can be used to search for correlations between the RP and the use of those optical components. We used the B Bessell filter for this investigation. While the amplitude of the signal is stronger in the U Bessell filter, there are many more twilight flats observed for the B Bessell, so we can achieve a more homogeneous angle distribution and a better signal-to-noise ratio. In Figures 9 – 12, the rotating structures are shown for different periods when the FORS instruments were mounted at the VLT units UT1 to UT4. The amplitudes of the structures are listed in Tab. 3, together with the combination of instrument, UT and LADC used in each case.

Inspection of the figures shows that the general structures frequently but not always change when any changes were made to the instrument. In most cases, these changes involve removing the instrument from the field rotator and remounting it. Slight changes in the optical alignment might therefore explain these differences. The overall shape of the RP seems to be more strongly correlated with the LADC than with either the UT or the instrument used. Structures observed with FORS1 and FORS2 look similar when the LADC A was used at UT2, UT3 or UT4. At UT1 with LADC A (Fig.9), both FORSs show a gradient of increasing flux from the lower left corner to the up-

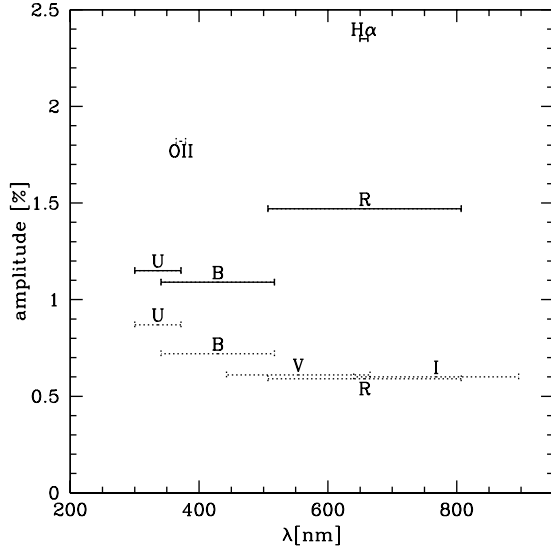


Fig. 7.— Amplitudes of the rotating pattern as a function of the wavelength range of the filters for the time ranges listed in Tab. 2. The FWHM filter width is shown for each filter, FORS1/2 data are marked by dotted lines and solid lines, respectively.

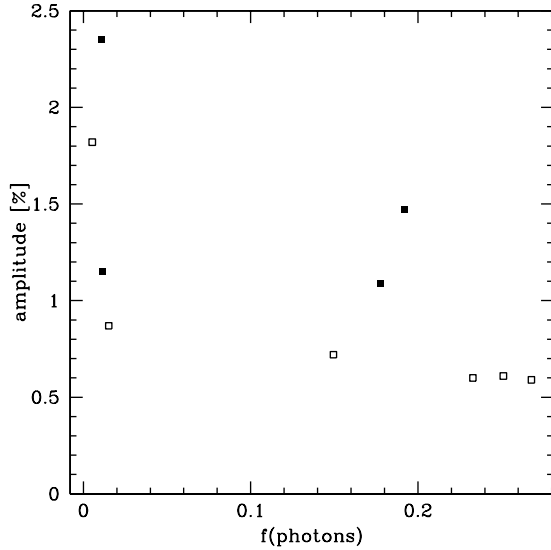


Fig. 8.— Amplitudes of rotating pattern as a function of the fraction of sky photons that pass through the filter. Different symbols are used for the two periods listed in Tab. 2, FORS1/2 data are distinguished by open and filled symbols, respectively.

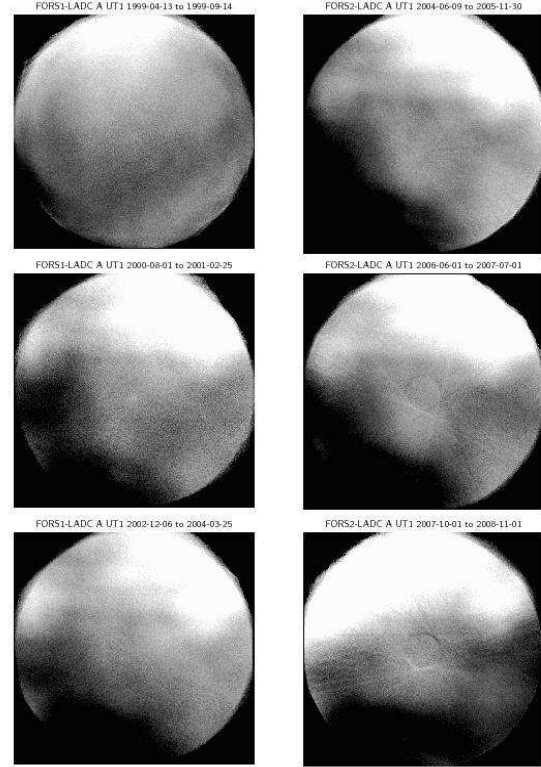


Fig. 9.— Comparison of flatfielded B_BESS twilight flat fields rotated to rotator angle 0 observed at UT1. The data on the left are from FORS1 (1999-04-13 to 1999-09-14, 2000-08-01 to 2001-02-25, and 2002-12-06 to 2004-03-25 from top to bottom). The data on the right are from FORS2 (2004-06-09 to 2005-11-30, 2006-06-01 to 2007-07-01, 2007-10-01 to 2008-11-01 from top to bottom). All images are displayed with cuts of 0.995 and 1.005.

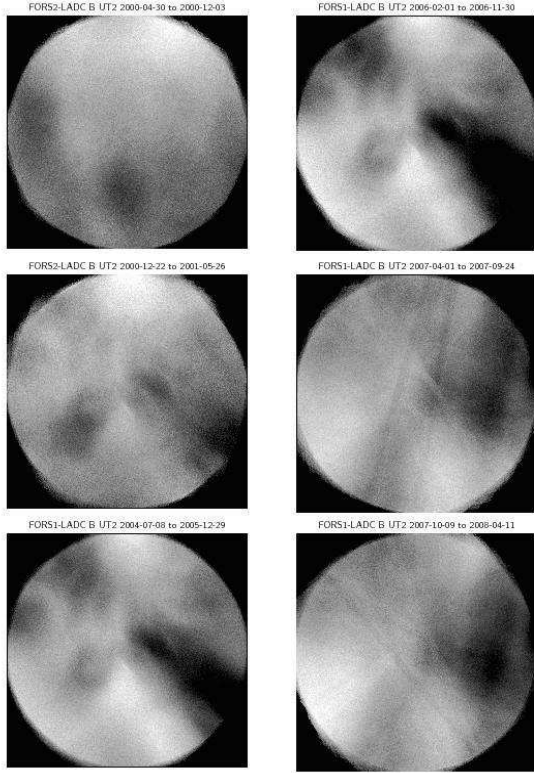


Fig. 10.— Same as in Fig. 9, but for UT2. The data on the left, top and center, are from FORS2 (2000-04-30 to 2000-12-03, 2000-12-22 to 2001-05-26 from top) The data on the bottom left and on the right are from FORS1 (bottom left: 2004-09-01 to 2005-12-29; right, top to bottom: 2006-02-01 to 2006-11-30, 2007-04-01 to 2007-09-24, 2007-10-09 to 2008-04-11).

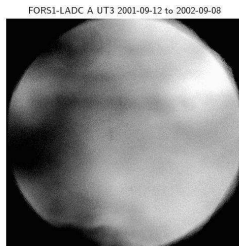


Fig. 11.— Same as in Fig. 9, but for UT3 (FORS1). The date range is 2001-09-12 to 2002-09-08.

per right corner for data observed after 1999. The amplitude of this effect increased when the LADC was switched from FORS1 to FORS2 (cf. Table 3). On the other hand, for UT2 and UT4 in combination with LADC B (Figs. 10 and 12) one can see the same features, a slanted “1”, in FORS1 data observed between July 2004 and December 2006 and in FORS2 data observed between December 2000 and May 2001 (UT2) and between June 2001 and October 2003 (UT4). A similar feature can be observed in the newest FORS1 data (since April 2007), although the “1” appears to be flipped and rotated. The feature is not present in the earliest FORS2 data at UT2, which look more similar to the FORS1 data from UT3 (Fig. 11) and show a slope similar to the UT1 data, albeit with some variation in the low flux region.

3.4. Contamination of the LADC

Under normal circumstances, the LADC is not accessible unless the FORS instrument is dismounted. After we identified the LADC as a possible cause for the RP, we visually inspected LADC B, which has been de-commissioned with FORS1 on March 31, 2009. Fig. 13 shows a picture of the lower prism illuminated with a flash light. Comparing the smudges seen in this picture to the structures visible in Figs. 6, 10, and 12 suggests that the LADC is responsible for a major part of these structures.

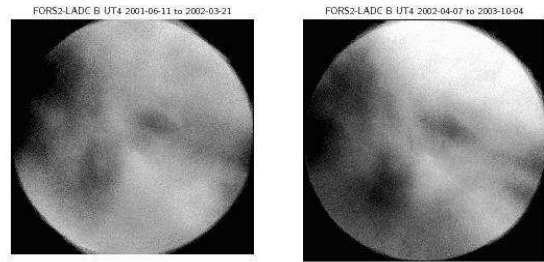


Fig. 12.— Same as in Fig. 9, but for UT4 (FORS2). The date ranges are 2001-06-11 to 2002-03-21 (left) and 2002-04-07 to 2003-10-04 (right).

4. Implications for Photometry

4.1. RP and Photometric Zeropoint Variations

The observed RP raises the question how accurate relative photometry can be obtained from FORS images. The obvious question is whether the RP is a faithful representation of throughput variations across the detector, or whether it is an additive defect in the flatfields that should be removed. To address this issues, we analyzed a set of dithered R-band observations of Stetson standard fields (Freudling et al. 2007a). Correlating the measured magnitudes of stars with features of the RP can determine whether the RP is additive or multiplicative, and thereby decide on the appropriate correction procedure.

The details of data taking and reduction are given in Freudling et al. (2007a,b,c). Here, we only give a brief summary. In total, 30 images of the field were taken on a 5×5 grid covering a total area of about $12' \times 12'$, including several rotations of the field. We removed any structure larger than 100 pixels from the masterflat, and the resulting masterflat was used to flatfield all the images. We then measured instrumental aperture magnitudes for any star that is included on at least two of the images. In total, there are about 10 000 measured magnitudes of 900 unique stars. The measured magnitudes were then used to fit a model of the illumination pattern, relative magnitude zero points of the stars and a zero point for each image. The model for the illumination pattern was a two-dimensional third order polynomial. The scales which can be fitted with such a model are too large to remove any possible sensitivity variations on the scales of the RP. We computed the residuals from the fit $\Delta m = m - m_{\text{st}} - m_i - i(x, y)$, where m are the measured instrumental magnitudes, m_{st} are the relative magnitudes of the stars, m_i the relative zero points of the images, and $i(x, y)$ is the model of the illumination pattern.

We then plotted these residuals with the corresponding pixel value of the normalized flatfields taken with the same rotator angle as the stellar images. The results are shown in left panel of Fig. 14. It can be seen that there is a correlation between the two quantities in the sense that measured magnitudes of the same stars are brighter when they are in areas where the RP is bright, and fainter

where the RP is faint. A line with a slope of -1 in Fig. 14 shows the expected relation if the RP directly represents sensitivity variations across the detector. The reduced χ^2_ν from this line is 1.45. This suggests that the RP is indeed a valid part of the flatfield, i.e. the pattern is multiplicative and is directly related to the photometry.

In order to evaluate the significance of this result, we repeated the described procedure with the positions of the stars on the detector randomly drawn. In this case, we do not expect any relation between the residuals and the values on the RP. Residuals from fitting a line with a slope -1 therefore will be large, and this can be detected by a large values for χ^2_ν . For each realization, we computed the χ^2_ν of the fit in the same way as we did with the original data. The distribution of χ^2_ν for 10 000 realizations is show in the right panel of Fig. 14. Only in about 0.2% of all realization was the χ^2_ν as low as for the original data. As an additional test, we repeated the procedure with the original data, but the RP rotated by 90° . Again, there was no correlation between the residuals and the RP. We therefore conclude that at least for the R_BESS filter we tested, the RP presents a sensitivity variation across the detectors.

However, as discussed in Sec. 3.2 we also see evidence for a scattered component which shows up relatively strongly for narrow band filters. Therefore, the RP for the narrow band filters might include both multiplicative and additive components.

4.2. Data Reduction Strategy

One consequence of the findings discussed here is that the RP will significantly affect the master flats unless the rotator angles are carefully controlled. Applying a flatfield that includes the RP to imaging data with a different rotator angle will introduce shifts of the photometric zeropoint with amplitudes twice as large as the RP, i.e. up to almost 4% across the inner circle on the detector for broad band filters. There are several conceivable strategies to address this problem. The first is to try to isolate the RP as we have described, rotate it to the rotator angle of each individual twilight flat, and correct the master flats. The disadvantage of this approach is that it is not applicable to the corners of the detectors where the RP cannot be isolated. The second strategy is to

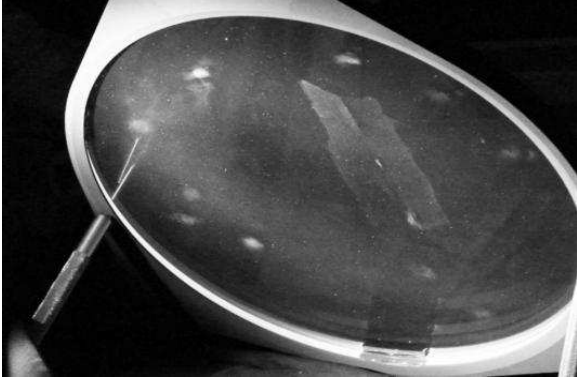


Fig. 13.— The lower prism of LADC B illuminated by a flashlight, photograph taken on 2009 Jun 29.

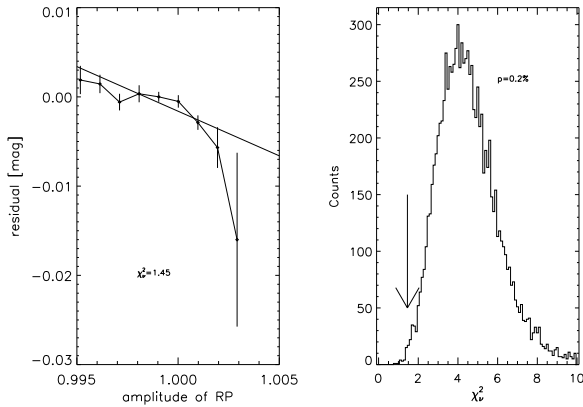


Fig. 14.— Left panel: Magnitude residuals as a function of pixel value of the RP. The data points are the averaged magnitude residuals for a given level of the RP, error bars are the 1σ uncertainties of the mean. The solid line is the fit of a line with a slope of -1 to the data points. The reduced χ^2 of the fit is 1.45. Right panel: Distribution of reduced χ^2 for 10 000 fits to residuals versus pixel values of the RP. The positions of the stars were randomly assigned for each each of the fits. The arrow marks the χ^2_{ν} of the original data as shown in the left panel.

remove any structure in the twilight flats on the scale of the structures seen in the RP (see Fig. 5), and then determine the larger scale illumination correction through independent observations. The disadvantage of this approach is that it is difficult to determine the illumination correction with sufficient spatial resolution. Finally, one could address the RP matching the orientation of flat fields to the corresponding science images. For reasons of efficiency, the implementation of such a strategy requires one to restrict the orientation of science data to the small number of selected rotator angles, for which flatfields are available. We consider this solution to be the best strategy.

We also recommend this strategy of searching for twilight flats with rotator angles close to those of the science data to users, who already have FORS data or retrieve them from the archive. They must, however, avoid mixing data across interventions. If there are no flat fields in the given time range with a rotator angle similar to that of the science data, the next best solution is to construct a master twilight flat by combining twilight observations with a large range of rotator angles to smear out the RP.

5. Summary and Conclusions

Using archived calibration data from more than eight years we have shown that the master twilight flats regularly produced from FORS observations include structures that are not related to sensitivity variations across the detector. Part of this is caused by field illumination effects, which can be corrected using standard field illumination correction (for details see Freudling et al. 2007a) but in addition we find a pattern which rotates with the setting of the field rotator. This pattern is stable in the absence of instrument interventions, but occasionally changes when work on the instrument has been performed.

Obviously the source of this additional pattern must be either partly or completely external to the instrument itself in order to be able to follow the field rotator. Possible candidates were therefore the guide probe or structures inside or on the M3 tower, e.g. reflections off some structure related to the M3 mirror or to the LADC. Alternatively the effect may be caused directly by transmission variations in the optical surfaces of the LADC it-

self. Since the method by which one would correct for the effect is very different for reflections (additive effect) or transmission variations (multiplicative), we have deemed it important to determine its source.

Data taken through a narrow band filter suggested at first that reflections were the main cause, but data taken through a second narrow band filter did not strongly support this suspicion. There is evidence that the rotating patterns followed the LADCs when they moved between the two instruments. Further a direct inspection of one of the LADCs, which has now been dismantled and decommissioned, showed a structure on its coating which well resembles the pattern seen in the flat fields. A last test finally showed that comparison to photometric stellar data confirmed that the pattern is multiplicative, i.e. consistent with transmission variations. Having thus identified the cause we conclude that if it is left uncorrected in the worst case it could cause systematic errors of up to 4% in the photometry. Future photometric observations with the FORS2 instrument will have to take this newly discovered feature into account in order to remove or minimize its impact. Several options for corrective action exist and are described in this paper in Sect. 4.2.

One might well expect that a similar detailed analysis of archived calibration data from other long-term-stable instrument/telescope configurations on alt/az mounted telescopes would produce similar results, in particular if these also include LADCs (e.g. LRIS on Keck). We recommend that such analysis should be performed on all instruments used for photometry as part of the general health check and trending analysis when sufficient calibration data are available. Such effects could be stronger or weaker on other instruments than were found here, and they could be both additive and multiplicative as described above. In this paper we have provided a detailed description of how such an analysis is best performed, how one may best determine the source of such effects, and how one may correct for them.

Acknowledgments: We thank Hans Dekker, Martino Romaniello, and Andreas Kaufer for valuable discussions. We highly appreciate the help of the staff on Paranal in locating and examining the LADC-B.

REFERENCES

- Avila, G., Rupprecht, G., Beckers, J. in: *Optical Telescopes of Today and Tomorrow*, ed. A. Ardeberg, Proc. SPIE 2871, p. 1135
- Andersen, M. I., Freyhammer, L. and Storm, J. 1995, in *Calibrating and Understanding HST and ESO Instruments*, ed. Benvenuti, Piero, Garching: ESO, p. 87.
- Freudling, W., Romaniello, M., Patat, F., Møller, P., Jehin, E. & O'Brien, K. 2007, *The Future of Photometric, Spectrophotometric and Polarimetric Standardization*, ed. C. Sterken, ASP Conf. Ser. 364, p. 113
- Freudling, W., Møller, P., Patat, F., et al. 2007, *The 2007 ESO Instrument Calibration Workshop*, ed Kaufer, A. & Kerber, F. (New York: Springer), p. 25
- Freudling, W., Møller, P., Patat, F., et al. 2007, *The Messenger*, 128, p. 13
- Fynbo, J. U., Moller, P. & Warren, S. J. 1999, *MNRAS*, 305, 849
- Koch, A., Odenkirchen, M., Grebel, E. K., & Caldwell, J. A. R. 2003 *Astronomische Nachrichten Supplement*, 324, 95
- Møller, P., Järvinen, A., Rupprecht, G., et al. 2005, *FORS: An assessment of obtainable photometric accuracy and outline for strategy for improvement*, VLT-TRE-ESO-13100-3808
- Patat, F., Ugolnikov, O. S. & Postlyakov, O. V. 2006, *A&A*, 455, 395

TABLE 1
COMBINATIONS OF TELESCOPE AND FORS

Instrument	Unit Telescope	start	end	time range used	event	# frames
FORS1	UT1-Antu	1999-04-01	2001-07-31	1999-04-13 ... 1999-09-14	1999-10-25 FORS1 maintenance	142
				2000-08-01 ... 2001-02-25	2001-03-25 mirror re-coating	137
	UT3-Melipal	2001-08-02	2002-10-19	2001-09-12 ... 2002-09-08	2002-10-19 move from UT3 to UT1	266
	UT1-Antu	2002-10-22	2004-05-30	2002-12-06 ... 2004-03-25	2004-06-04 move from UT1 to UT2	234
	UT2-Kueyen	2004-06-06	2009-03-31	2004-09-01 ... 2005-12-29	2006-01-27 FORS1 maintenance	247
				2006-02-01 ... 2006-11-30	2006-12-01 mirror recoating	201
				2007-04-01 ... 2007-09-24	2007-04-01 new CCD mosaic	46/106/134/127/129/141
					2007-09-24 FORS1 maintenance	(OII/U/B/V/R/I)
				2007-10-09 ... 2008-04-11	2008-04-11 b ₁ HIGH replaces B ₁ BESS as standard filter	132
FORS2	UT2-Kueyen	2000-03-25	2001-06-01	2000-03-30 ... 2000-12-03	2000-12-08 FORS2 maintenance	155
				2000-12-22 ... 2001-05-26	2001-06-02 move from UT2 to UT1	125
	UT4-Yepun	2001-06-05	2004-05-29	2001-06-11 ... 2002-03-21	2002-03-29 new CCD mosaic	199
				2002-04-07 ... 2003-10-04	2004-05-31 move from UT4 to UT1	289
	UT1-Antu	2004-06-06		2004-06-09 ... 2005-11-30	2005-12-15 mirror recoating	256
				2006-06-01 ... 2007-07-01	2007-07-02 mirror recoating	154
				2007-10-01 ... 2008-11-01	2008-11-06 mirror recoating	187

TABLE 2
 AMPLITUDE OF THE ROTATOR EFFECT WITH WAVELENGTH AND BANDWIDTH FOR FORS1@UT2
 (2007-04-01 ... 2007-09-24) AND FORS2@UT4 (2002-04-07 ... 2003-10-04)

Filter	Central Wavelength (nm)	FWHM (nm)	amplitude (%)
FORS1			
U_BESSELL	336.0	36.0	0.87
OII	371.7	7.3	1.82
B_BESSELL	429.0	88.0	0.72
V_BESSELL	554.0	111.5	0.61
R_BESSELL	657.0	150.0	0.60
I_BESSELL	768.0	138.0	0.61
FORS2			
U_SPECIAL	362.0	29.0	1.15
B_BESSELL	429.0	88.0	1.09
R_SPECIAL	655.0	165.0	1.47
H $_{\alpha}$	656.3	6.1	2.35

TABLE 3
AMPLITUDE OF THE ROTATOR EFFECT WITH TELESCOPE-INSTRUMENT-LADC COMBINATION

Instrument	Unit Telescope	time range used	amplitude (%)	features	LADC
FORS1	UT1-Antu	1999-04-13 ... 1999-09-14	1.04	—	A
FORS1	UT1-Antu	2000-08-01 ... 2001-02-25	1.73	slope	A
FORS1	UT1-Antu	2002-12-06 ... 2004-03-25	1.75	slope	A
FORS2	UT1-Antu	2004-06-09 ... 2005-11-30	1.96	slope	A
FORS2	UT1-Antu	2006-06-01 ... 2007-07-01	2.03	slope	A
FORS2	UT1-Antu	2007-10-01 ... 2008-11-01	1.97	slope	A
FORS2	UT2-Kueyen	2000-04-30 ... 2000-12-03	0.72	“spotty slope”	B
FORS2	UT2-Kueyen	2000-12-22 ... 2001-05-26	0.87	slanted “1”	B
FORS1	UT2-Kueyen	2004-07-08 ... 2005-12-29	0.97	slanted “1”	B
FORS1	UT2-Kueyen	2006-02-01 ... 2006-11-30	0.72	slanted “1”	B
FORS1	UT2-Kueyen	2007-04-01 ... 2007-09-24	1.19	slanted “1”, flipped	B
FORS1	UT2-Kueyen	2007-10-09 ... 2008-04-11	0.90	slanted “1”, flipped	B
FORS1	UT3-Melipal	2001-09-12 ... 2002-09-08	1.04	“spotty slope”	A
FORS2	UT4-Yepun	2001-06-11 ... 2002-03-21	0.87	slanted “1”	B
FORS2	UT4-Yepun	2002-04-07 ... 2003-10-04	1.10	slanted “1”	B